FORCE-DISPLACEMENT RELATIONSHIPS OF A TENSEGRITY STRUCTURE CONSIDERING BAR INTERFERENCE

Min LIN[1], Tuanjie LI[2], Zhifei JI[3], Mingkui CHE[4]

Tensegrity systems are proposed to be used in several disciplines due to their advantages. The force-displacement relationships play an important role for their applications. However, few developments are found to study the force-displacement relationship considering the bars' interference. In this work, we compute the force-displacement relationships by using the Lagrangian formulation considering the bars' interference. Afterwards, we have made an experimental prototype. The force-displacement relationships obtained by experiments are compared with those computed from the energy-based constraint equations. Finally, the evolution of the external force has been researched along with the evolution of the stiffnesses of the springs.

Keywords: Tensegrity; Energy formulation; Bar interference; Force-displacement relationship;

List of symbols

$\boldsymbol{q}$: Vector of generalized coordinates; L: Length of rigid bars
K: Spring constant; L_{01}, l_{02}: Rest lengths of springs
$\boldsymbol{f}_{nc}$: Vector of generalized non-conservative forces
U: Potential energy of the system
T: kinetic energy of the system; m: Mass of the bars

1. Introduction

Tensegrity systems are formed by a combination of rigid components (bars) in compression and compliant components (springs or cables) in tension. These systems have advantages of light-weight, deployability, deformability, etc. Due to these characteristics, they have been proposed to be applied in many fields, such as domes [1-4], bridges [5-6], sensors [7], antennas [8-9], mobile robots [10-11], mechanisms [12-14] and water wave energy harvesters [15].

[1] Ph. D candidate, School of Electro-Mechanical Engineering, Xidian University, CHINA, e-mail: structmlin@163.com
[2] School of Electro-Mechanical Engineering, Xidian University, CHINA, e-mail: tjli888@126.com
[3] Corresponding author. College of Mechanical and Energy Engineering, Jimei University, CHINA, e-mail: zfji18@163.com
[4] School of Electro-Mechanical Engineering, Xidian University, CHINA, e-mail: 1390740721@qq.com

The investigation of tensegrity systems can be divided into two branches. One is the study of statics, and the other is the study of dynamic behaviors. For the statics of tensegrity systems, an important issue, named form-finding, has been dealt with by many researchers [16]. Masic et al. [17] proposed an algebraic-based method to deal with the form-finding of symmetric tensegrity structures. Pagitz and Tur [18] developed finite element based form-finding method for tensegrities. More recently, optimization algorithms have been proposed to find the shape of large irregular tensegrities. Moreover, a review of form-finding methods was provided by Juan and Tur [19].

The investigations of dynamics of tensegrities are mainly focused on the force-displacement relationship. This relationship is essential to understand how the structure behaves when subjected to external perturbations as well as to find out the new stable configuration under such conditions. This study has been carried out from two points of view. First, considering the structure is at an arbitrary position and may experience large deformations. Second, considering the structure is at an equilibrium configuration and can only experience small perturbations around it.

When tensegrities experience large deformations, more general methods use either the Newtonian or Lagrangian formulation to get force-displacement relationships which are valid in any configurations. Kanchanasaratool and Williamson [20] studied a 6-bar tensegrity platform using Newtonian formulation. Skelton et al. [21] found a simplified model of the Newtonian formulation for class-1 tensegrity shell. Motro et al. [22] performed the study on how tensegrity structures dynamically behave when external loads are applied on the structure nodes using Lagrangian formulation. Murakami [23] used the Lagrangian method to model the dynamic behavior of a tensegrity structure taking into account additional non-linear effects, such as the deformability of the structure edges and the non-linear elasticity of the tensional members. When tensegrities experience small perturbations, they can be considered to be at equilibrium configuration. In this case, it does not take into account any dynamics, instead, only the geometry of the tensegrity around an equilibrium position is used to find out the force-displacement relationship. Oppenheim and Williams [24] proposed a method which takes into account the fact that all equilibrium configurations have minimum energy. To the best of our knowledge, few researchers studied the force-displacement problem considering the bars' interference which may occur and be of significance in the real world.

A recursive matrix approach [25] was developed to model the kinematics and dynamics of parallel mechanisms. In this paper, an adaptation of the method of matrix approach is used to deal with the kinematics of the tensegrity structure.

In this paper, we studied the force-displacement relationship of a tensegrity considering the interference between bars. The main contribution of

this article is threefold. First, by using Lagrangian formulation, we give the constraint equations representing the force-displacement relationship of a tensegrity structure. The equations have been solved by the Newton-Raphson approach. Second, the interference between the bars is discussed explicitly to determine the maximum of the applied force. Third, we have made an experimental prototype to certify the correctness of the obtained force-displacement relationship.

2. Structure description

The tensegrity structure considered here is shown in Figure 1(a). It consists of three compressive components and six tensile components. The compressive components are bars of length L joining node pairs A_iB_i while the tensile components are springs joining node pairs $A_iB_{i+1}$and B_iB_{i+1}, (i = 1, 2, 3 with i +1 = 1 if i = 3). The structure was firstly researched by Oppenheim and Williams [24] by making the symmetric hypothesis. In this work, we completed the analysis of force-displacement relationships without the symmetric hypothesis.

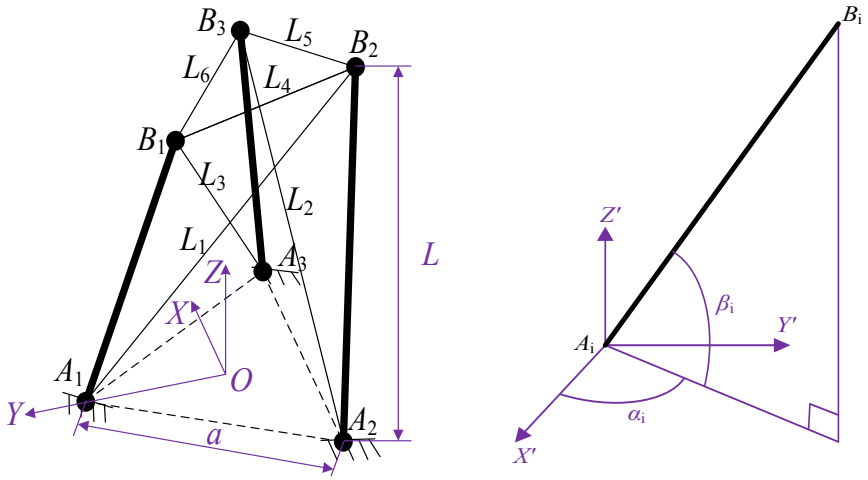

(a) (b)

Fig. 1 Simple tensegrity structure

A fixed reference frame is located at the center of the triangle $A_1A_2A_3$, denoted by node O, with its Y axis directed toward node A_1 and its Z axis perpendicular to the plane $A_1A_2A_3$.

The vectors specifying the position of nodes A_i and B_i in this reference frame are defined as a_i and b_i, respectively. The bars of mass m have the following length

$$L = \sqrt{\left(\boldsymbol{b}_i - \boldsymbol{a}_i\right)^T \left(\boldsymbol{b}_i - \boldsymbol{a}_i\right)} \tag{1}$$

The orientation of bar i relative to the fixed reference frame will be represented by angles α_i and β_i as illustrated in Figure 1 (b). In this figure, the reference frame $X'Y'Z'$ is located at node A_i and have the same orientation as frame XYZ. The bars are attached with spherical joints to node A_i. Vectors $\boldsymbol{a}_i$ take the following forms:

$$\begin{aligned} \boldsymbol{a}_1 &= [0 \ a/(3^{0.5}) \ 0]^{\mathrm{T}} \\ \boldsymbol{a}_2 &= [\hat{a}0.5a \quad \hat{a} \ 0.5a/(3^{0.5}) \ \ 0]^{\mathrm{T}} \\ \boldsymbol{a}_3 &= [0.5a \ \ \hat{a}0.5a/3^{0.5} \ 0]^{\mathrm{T}} \end{aligned} \tag{2}$$

Furthermore, from Figure 1 (b), it can be seen that

$$\boldsymbol{b}_i = \boldsymbol{a}_i + L\boldsymbol{R}_{1i}\boldsymbol{R}_{2i}\boldsymbol{T}_{u1}, \ \ (i = 1,2,3) \tag{3}$$

with $\boldsymbol{R}_{0\mathrm{i}}$ = rot(z, $\hat{I}_i$), $\boldsymbol{R}_{1\mathrm{i}}$ = rot(z, $\hat{I}\pm i$), $\boldsymbol{R}_{2\mathrm{i}}$ = rot(y, $\hat{I}^2 i$), $u_1=[1 \ \ 0 \ \ 0]^{\mathrm{T}}$ and $a_{\mathrm{i}}=\{a/3^{0.5}\}\boldsymbol{R}_{0\mathrm{i}}u_1$.

We obtain

$$\boldsymbol{b}_i = \left\{a / 3^{0.5}\right\}\left[\cos\hat{\mathrm{I}}_i \quad \sin\hat{\mathrm{I}}_i \quad 0\right]^T + L\left[\cos\hat{\mathrm{I}}\pm i\cos\hat{\mathrm{I}}_i^2 \quad \sin\hat{\mathrm{I}}\pm i\cos\hat{\mathrm{I}}_i^2 \quad \sin\hat{\mathrm{I}}_i^2\right]^T \tag{4}$$

where $\hat{I}_1$=Ï/2, $\hat{I}_2$=â5Ï/6 and $\hat{I}_3$= âÏ/6.

All the springs are assumed to be massless and linear with stiffness K. Moreover, springs A_iB_{i+1} have the same free length L_{01} while springs B_iB_{i+1} have the same free length L_{02} (i = 1, 2, 3 with i +1 = 1 if i = 3). The stiffnesses of the bars are considered to be infinite relative to those of the springs.

From the above description of the structure, it can be observed that only six generalized coordinates are needed to describe the configuration of the structure. These generalized coordinates are thus chosen as $\boldsymbol{q}$ = $[q_1, q_2, q_3, q_4, q_5, q_6]^{\mathrm{T}} = [\alpha_1, \alpha_2, \alpha_3, \beta_1, \beta_2, \beta_3]^{\mathrm{T}}$.

3. Response of the structure to external loads

The external force applied on node B_i is denoted by $\boldsymbol{F}_i = [F_{ix} \ F_{iy} \ F_{iz}]^{\mathrm{T}}$ (F_{ix} represents the component of the force $\boldsymbol{F}_i$ along the X axis, etc.). When a bar interferes with another in a structure, it will not be in tensegrity configurations. In this section, Lagrangian formulation is used to find the force-displacement relationship considering bars' interference.

3.1 Constraint equations for force-displacement relationships

According to the Lagrangian formulation, the dynamic model of the structure can be written as:

$$\frac{d}{dt}\frac{\partial T}{\partial \dot{\boldsymbol{q}}} - \frac{\partial T}{\partial \boldsymbol{q}} + \frac{\partial U}{\partial \boldsymbol{q}} = \boldsymbol{f}_{nc} \tag{5}$$

Where T and U are the kinetic and potential energies of the system, $\boldsymbol{q}$ = $[\alpha_1, \alpha_2, \alpha_3, \beta_1, \beta_2, \beta_3]^{\mathrm{T}}$ is the vector of generalized coordinates and $\boldsymbol{f}_{\mathrm{nc}}$ = $[f_{\mathrm{nc1}}, f_{\mathrm{nc2}}, f_{\mathrm{nc3}}, f_{\mathrm{nc4}}, f_{\mathrm{nc5}}, f_{\mathrm{nc6}}]^{\mathrm{T}}$ is the vector of generalized non-conservative forces acting on the system. Since this paper mainly deals with the case that the structure can only experience

small perturbations, the structure can be always considered to be at equilibrium configurations. It follows that the kinetic energy U is always equal to zero. Considering this fact, Eq. (4) can be rewritten as

$$\frac{\partial U}{\partial \mathbf{q}} = \boldsymbol{f}_{nc} \tag{6}$$

Eq. (5) represents the relationship between external forces and the generalized coordinates. Let $\boldsymbol{F}_i = [F_{ix},\ F_{iy},\ F_{iz}]^{\mathrm{T}}$ be the force applied at the node B_i, the non-conservative components of generalized forces can be derived as:

$$\begin{aligned} f_{inc1} &= L\boldsymbol{u}_3^{T}\boldsymbol{R}_{2i}\boldsymbol{T}_{\tilde{A}''1}\boldsymbol{R}_{2i}\boldsymbol{R}_{1i}T\boldsymbol{F}_i \\ f_{inc2} &= -L\boldsymbol{u}_2^{T}\boldsymbol{R}_{2i}\boldsymbol{T}_{\tilde{A}''1}\boldsymbol{R}_{2i}\boldsymbol{R}_{1i}\boldsymbol{T}\boldsymbol{F}_i \\ \boldsymbol{u}_2^{T} &= [0 \quad 1 \quad 0]^{\mathrm{T}},\ \boldsymbol{u}_3^{T} = [0 \quad 0 \quad 1]^{\mathrm{T}},\ (i = 1,\ 2,\ 3) \end{aligned} \tag{7}$$

where $\tilde{A}''1$ is the skew-symmetric matrix associated to unit vector $\boldsymbol{u}_1$. We obtain following six analytical expressions:

$$f_{nc1} = -F_{1x}L\cos\beta_1\sin\alpha_1 + F_{1y}L\cos\beta_1\cos\alpha_1 \tag{8}$$

$$f_{nc2} = -F_{1x}L\sin\beta_1\cos\alpha_1 - F_{1y}L\sin\beta_1\sin\alpha_1 + F_{1z}L\cos\beta_1 \tag{9}$$

$$f_{nc3} = -F_{2x}L\cos\beta_2\sin\alpha_2 + F_{2y}L\cos\beta_2\cos\alpha_2 \tag{10}$$

$$f_{nc4} = -F_{2x}L\sin\beta_2\cos\alpha_2 - F_{2y}L\sin\beta_2\sin\alpha_2 + F_{2z}L\cos\beta_2 \tag{11}$$

$$f_{nc5} = -F_{3x}L\cos\beta_3\sin\alpha_3 + F_{3y}L\cos\beta_3\cos\alpha_3 \tag{12}$$

$$f_{nc6} = -F_{3x}L\sin\beta_3\cos\alpha_3 - F_{3y}L\sin\beta_2\sin\alpha_3 + F_{3z}L\cos\beta_3 \tag{13}$$

From Eqs. (2)-(3), it can be seen that the coordinates of nodes A_i and B_i can be expressed in terms of the generalized coordinates. Furthermore, the lengths of the springs in the system can be easily expressed as a function of α_1, α_2, α_3, β_1, β_2 and β_3. The potential energy thus becomes

$$U = 0.5\hat{I}\pounds + 0.5\ \hat{I}\pounds + 0.5\mathrm{mg}L\ \hat{I}\pounds\sin\hat{\Gamma}^2{}_i \tag{14}$$

where g is the acceleration due to gravity. Variables L_i (i = 1, 2, …, 6) in the above equation are detailed in Appendix A. By substituting Eqs. (6)-(11) and (12) into Eq. (5), we obtain

$$2K\left[\sum_{i=1}^{3}(L_{\mathrm{i}} - L_{01})\frac{\partial L_{\mathrm{i}}}{\partial \alpha_1} + \sum_{i=4}^{6}(L_{\mathrm{i}} - L_{02})\frac{\partial L_{\mathrm{i}}}{\partial \alpha_1}\right] + F_{1x}L\cos\beta_1\sin\alpha_1 - F_{1y}L\cos\beta_1\cos\alpha_1 = 0 \tag{15}$$

$$\begin{aligned} &2K\left[\sum_{i=1}^{3}(L_{\mathrm{i}} - L_{01})\frac{\partial L_{\mathrm{i}}}{\partial \beta_1} + \sum_{i=4}^{6}(L_{\mathrm{i}} - L_{02})\frac{\partial L_{\mathrm{i}}}{\partial \beta_1}\right] + \frac{mgL}{2}\cos\beta_1 \\ &+ F_{1x}L\sin\beta_1\cos\alpha_1 + F_{1y}L\sin\beta_1\sin\alpha_1 - F_{1z}L\cos\beta_1 = 0 \end{aligned} \tag{16}$$

$$2K\left[\sum_{i=1}^{3}(L_{\mathrm{i}} - L_{01})\frac{\partial L_{\mathrm{i}}}{\partial \alpha_2} + \sum_{i=4}^{6}(L_{\mathrm{i}} - L_{02})\frac{\partial L_{\mathrm{i}}}{\partial \alpha_2}\right] + F_{2x}L\cos\beta_2\sin\alpha_2 - F_{2y}L\cos\beta_2\cos\alpha_2 = 0 \tag{17}$$

$$2K\left[\sum_{i=1}^{3}(L_{\mathrm{i}}-L_{01})\frac{\partial L_{\mathrm{i}}}{\partial \beta_2}+\sum_{i=4}^{6}(L_{\mathrm{i}}-L_{02})\frac{\partial L_{\mathrm{i}}}{\partial \beta_2}\right]+\frac{mgL}{2}\cos\beta_2 + F_{2x}L\sin\beta_2\cos\alpha_2+F_{2y}L\sin\beta_2\sin\alpha_2-F_{2z}L\cos\beta_2=0 \tag{18}$$

$$2K\left[\sum_{i=1}^{3}(L_{\mathrm{i}}-L_{01})\frac{\partial L_{\mathrm{i}}}{\partial \alpha_3}+\sum_{i=4}^{6}(L_{\mathrm{i}}-L_{02})\frac{\partial L_{\mathrm{i}}}{\partial \alpha_3}\right]+F_{3x}L\cos\beta_3\sin\alpha_3-F_{3y}L\cos\beta_3\cos\alpha_3=0 \tag{19}$$

$$2K\left[\sum_{i=1}^{3}(L_{\mathrm{i}}-L_{01})\frac{\partial L_{\mathrm{i}}}{\partial \beta_3}+\sum_{i=4}^{6}(L_{\mathrm{i}}-L_{02})\frac{\partial L_{\mathrm{i}}}{\partial \beta_3}\right]+\frac{mgL}{2}\cos\beta_3 + F_{3x}L\sin\beta_3\cos\alpha_3+F_{3y}L\sin\beta_2\sin\alpha_3-F_{3z}L\cos\beta_3=0 \tag{20}$$

By using Eqs. (13)-(18), the generalized coordinates $\boldsymbol{q}$ can be computed for a set of given external forces. This means that the force-displacement relationship of the structure can be obtained by solving Eqs. (13)-(18).

3.2 Bars' interference

Bars' interference might occur in the real world due to the fact that bars have physical dimensions. It is supposed that the bars are cylindrical with a diameter D. Then, the shortest distance between the center lines of two adjacent bars is denoted by D_i (i = 1, 2, 3). When two bars interfere, the following conditions should be satisfied.

$$D_i \le D \tag{21}$$

The unit vector in the direction of the common normal between two bar vectors $\boldsymbol{L}_i$ and $\boldsymbol{L}_{i+1}$, denoted by $\boldsymbol{n}_i$, can be written as

$$\boldsymbol{n}_i=\frac{\boldsymbol{L}_i\times\boldsymbol{L}_{i+1}}{\left|\boldsymbol{L}_i\times\boldsymbol{L}_{i+1}\right|} \tag{22}$$

The shortest distance between the two lines defined by the vectors $\boldsymbol{L}_i$ and $\boldsymbol{L}_{i+1}$, denoted by Δ_i, is given by

$$\Delta_i=\left|\boldsymbol{n}_i\left(\boldsymbol{a}_{i+1}-\boldsymbol{a}_i\right)\right| \tag{23}$$

Generally, the shortest distance between bars (D_i) is not equal to the shortest distance between the bar vectors (Δ_i). The relationship between the two depends on the location of the intersection points (C_i and C_{i+1}) of the bar vectors $\boldsymbol{L}_i$, $\boldsymbol{L}_{i+1}$ with their common normal $\boldsymbol{n}_i$. The coordinates of C_i can be computed by

$$\boldsymbol{c}_i=\boldsymbol{a}_i+\left|\frac{\left(\boldsymbol{a}_{i+1}-\boldsymbol{a}_i\right)\cdot\boldsymbol{m}_i}{\left(\boldsymbol{b}_i-\boldsymbol{a}_i\right)\cdot\boldsymbol{m}_i}\right|\left(\boldsymbol{b}_i-\boldsymbol{a}_i\right) \tag{24}$$

where $\boldsymbol{m}_i$ is a vector given by:

$$\boldsymbol{m}_i=\boldsymbol{n}_i\times\left(\boldsymbol{b}_{i+1}-\boldsymbol{a}_{i+1}\right) \tag{25}$$

Similarly for $\boldsymbol{c}_{i+1}$. In order to discuss the cases of bars' interference explicitly, two ancillary planes, denoted by S_1 and S_2, are introduced. S_1 is the plane where $\boldsymbol{L}_{i+1}$ is located and its normal vector is parallel to $\boldsymbol{n}_i$. Moreover, the normal vector of S_2 is also parallel to $\boldsymbol{n}_i$ and $\boldsymbol{L}_i$ is located on S_2. E_i is the projection of node B_{i+1} on the line defined by vector $\boldsymbol{L}_i$. E_{i+1} is the projection of node B_i on the line defined by vector $\boldsymbol{L}_{i+1}$. According to the location of C_i and C_{i+1}, three different cases need to be distinguished:

Case 1: Both intersection points are on the bars

In this case, as shown in Figure 2 (a), $D_i = \Delta_i$, and interference occurs if $D_i > \Delta_i$.

Case 2: One of the intersection points is outside the bar.

As shown in Figure 2 (b), if C_i is located beyond B_i, but C_{i+1} and E_{i+1} is on the (i+1)th bar, then D_i, which is the distance from B_i to the (i+1)th bar, is given by:

$$D_i = \frac{\left|\left(\boldsymbol{b}_i - \boldsymbol{a}_{i+1}\right) \times \boldsymbol{L}_{i+1}\right|}{\left|\boldsymbol{L}_{i+1}\right|} \tag{26}$$

As shown in Figure 2(c), if C_i is located beyond B_i, but C_{i+1} is on the (i+1)th bar with E_{i+1} not on the (i+1)th bar, then D_i, which is the distance from B_i to the (i+1)th bar, is given by:

$$D_i = \left|\boldsymbol{b}_i - \boldsymbol{a}_{i+1}\right| \tag{27}$$

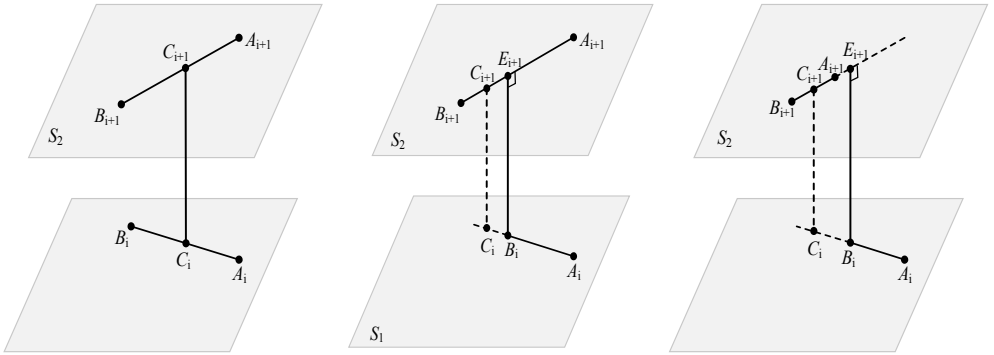

(a) (b) (c)

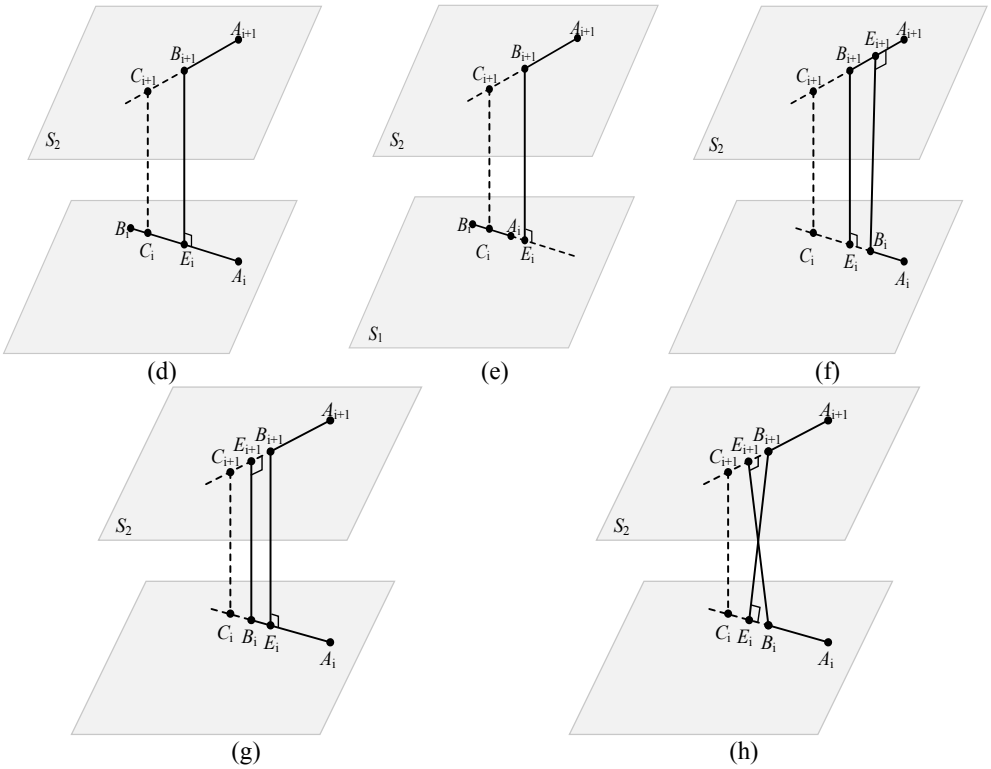

Fig. 2 Different cases of bars' interference

If C_{i+1} is located beyond B_{i+1}, but C_i and E_i is on the ith bar as shown in Figure 2(d), then D_i, which is the distance from B_{i+1} to the ith bar, is given by

$$D_i = \frac{\left|\left(\boldsymbol{b}_{i+1} - \boldsymbol{a}_i\right) \times \boldsymbol{L}_i\right|}{\left|\boldsymbol{L}_i\right|} \tag{28}$$

If C_{i+1} is located beyond B_{i+1}, but C_i is on the ith bar with E_i not on the ith bar as shown in Figure 2(e), then D_i, which is the distance from B_{i+1} to the ith bar, is given by

$$D_i = \left|\boldsymbol{b}_{i+1} - \boldsymbol{a}_i\right| \tag{29}$$

Case 3: Both intersection points are not on the bars

In this case, as shown in Figure 2(f-h), D_i depends on the location of E_i. There are three possibilities:

(1) If E_{i+1} is located on the bar $B_{i+1}A_{i+1}$ while E_i is out of the bar B_iA_i, as shown in Figure 2(f), then D_i is given by Eq. (24).

(2) If E_i is located on the bar B_iA_i while E_{i+1} is out of the bar $B_{i+1}A_{i+1}$, as shown in Figure 2(g), then D_i is given by Eq.(26).

(3) If both E_i and E_{i+1} are located out of the bars, as shown in Figure 2(h), then D_i is the distance between two joints B_i and B_{i+1}.

4. Experiments

4.1 Experimental prototype

The experimental prototype is shown in Figure 3. Carbon fiber tubes are used for the bars whose inside and outside diameters are 0.006 m and 0.008 m respectively. The length of bars are chosen as L = 0.578 m. The density of carbon fiber is $\rho = 1.8 \times 10^3$ kg/m^3. The mass of a bar in the structure can be computed as

$$m = \frac{\rho\pi\left(D^2 - d^2\right)L}{4} \tag{30}$$

where D and d denote the outside and inside diameters respectively. The rest length of side springs (springs A_1B_2, A_2B_3 and A_3B_1) is 0.336 m while the rest length of the top springs (springs B_1B_2, B_2B_3 and B_3B_1) is 0.356 m. Moreover, the spring constant is 173.2 N/m. In Figure 3, the sides of the fixed platform, denoted by $A_1A_2A_3$, are 0.41 m long. Moreover, calipers with accuracy of 0.1 mm are used to measure the current length of the springs. Since the rest lengths of springs are known, their extensions can be easily computed. Generally, when an external force is applied on the node B_i, the prototype will generate deformations. During this process, energy will be stored in the springs. The increased energy of the system can be represented by the extensions of the springs which are measured by the calipers. From Section 3.1, we know that the force-displacement relationship can be represented by the relationship between the external forces and the generalized coordinates. However, in the real world, the generalized coordinates are difficult to measure. Therefore, in the experiments, we try to reveal the force-displacement relationship of the prototype by using the relationship between the external force and the extensions of the springs.

Fig. 3 Experimental prototype

4.2 Main results

In the experiments, we only studied the cases that only one force ($\boldsymbol{F}_3$) is exerted on node B_3 along the Z axis. However, the method used in this work can be applied to the case that the external force is exerted on any node of the structure in any direction. By increasing the force from 0 N to 10 N, we obtained the lengths of the springs which are measured by calipers. Then, the corresponding extensions of the springs can be computed as shown in Table 1.

Table 1

Extensions of the springs obtained by experiments

F_{3z}/N	ΔL_1/mm	ΔL_2/mm	ΔL_3/mm	ΔL_4/mm	ΔL_5/mm	ΔL_6/mm
0	32.5988	32.1836	31.4954	50.9270	52.9330	48.5386
-1	33.084	34.0658	31.8073	51.0543	54.8730	44.2030
-2	34.2044	35.8326	32.0441	51.2912	56.9919	40.5982
-3	36.0226	38.3626	32.2730	51.5185	59.1224	37.0855
-4	37.0640	40.7714	32.4363	52.0554	61.4896	33.2460
-5	38.0762	43.7000	32.6557	53.0155	63.8568	28.9545
-6	39.5940	46.2817	32.9000	53.6815	67.2633	24.9076
-7	41.0598	47.4249	33.0083	54.0226	69.5150	22.4607
-8	42.0945	48.8453	33.2185	54.2254	72.5750	17.2679
-9	43.0469	52.7333	33.4594	54.4337	75.3464	13.6363
-10	44.0208	54.8176	33.8072	54.6998	78.4065	10.3799

In Table 1, ΔL_i is the extension of the spring i, as shown in Figure 1(a). Furthermore, ΔL_i can also be computed from Eqs. (13)-(18) for a set of given external forces by using the Newton-Raphson algorithm, as shown in Table 2.

Table 2

Extensions of the springs computedfromEqs. (13)-(18)

F_{3z}/N	ΔL_1/mm	ΔL_2/mm	ΔL_3/mm	ΔL_4/mm	ΔL_5/mm	ΔL_6/mm
0	31.3242	31.3212	31.3173	50.5953	50.5881	50.590840
-1	32.3180	33.1572	31.4903	50.9329	52.5784	46.494939
-2	33.3551	35.1283	31.6627	51.2700	54.6671	42.388409
-3	34.4389	37.2472	31.8372	51.6082	56.8603	38.277880
-4	35.5729	39.5262	32.0175	51.9496	59.1638	34.170881
-5	36.7614	41.9789	32.2083	52.2970	61.5835	30.075916
-6	38.0090	44.6188	32.4163	52.6535	64.1249	26.002510
-7	39.3212	47.4593	32.6494	53.0230	66.7930	21.961228
-8	40.7040	50.5131	32.9180	53.4100	69.5916	17.963650
-9	42.1642	53.7913	33.2343	53.8184	72.5232	14.022284
-10	43.7094	57.3025	33.6127	54.2537	75.5889	10.150407

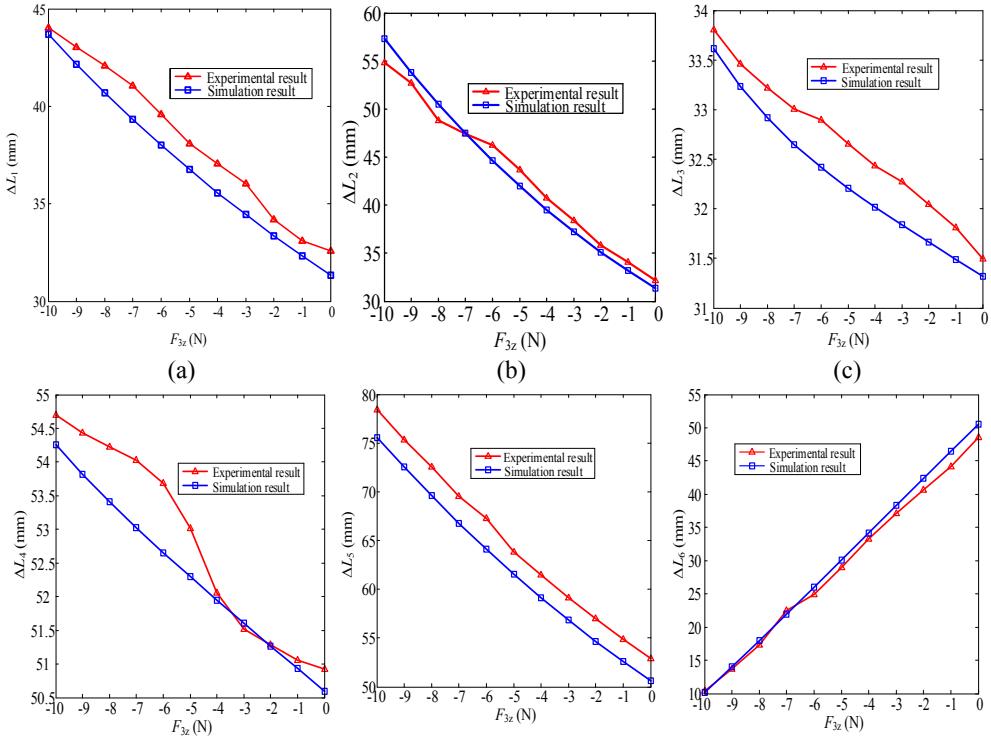

Fig. 4 Variations of the spring extensions along with the external force

Here, it is interesting to study the relationship between the external force F_{3z} and the extensions ΔL_i. This relationship obtained from Eqs. (13)-(18) is compared with that obtained from experiments. From Figure 4 (a-f), it can be seen that the law how the extensions ΔL_i vary over the external force is almost linear. This fact can be tested by experimental and theoretical results respectively. Furthermore, the force-displacement relationships obtained by Eqs. (13)-(18) are quite agree with experimental results. Let ΔL_{ie}, obtained by experiments, denote the extension of spring i, and ΔL_{is} denote the extension of spring i computed from Eqs. (13)-(18), the relative error is defined as

$$e_i = \frac{\left|\Delta L_{is} - \Delta L_{ie}\right|}{\Delta L_{is}} \tag{31}$$

The relative errors between the experimental and theoretical results can be computed by Eq. (29), shown in Table 3.

Table 3

Relative errors between the experimental and theoretical results

F_{3z}/N	e_1	e_2	e_3	e_4	e_5	e_6
0	4.07%	2.75%	0.57%	0.66%	4.64%	4.06%
-1	2.37%	2.74%	1.01%	0.24%	4.36%	4.93%
-2	2.55%	2.00%	1.21%	0.04%	4.25%	4.22%
-3	4.59%	2.99%	1.37%	0.17%	3.98%	3.12%
-4	4.19%	3.15%	1.31%	0.20%	3.93%	2.71%
-5	3.58%	4.10%	1.39%	1.37%	3.69%	3.73%
-6	4.17%	3.73%	1.49%	1.95%	4.89%	4.21%
-7	4.42%	0.07%	1.10%	1.89%	4.08%	2.27%
-8	3.42%	3.30%	0.91%	1.53%	4.29%	3.87%
-9	2.09%	1.97%	0.68%	1.14%	3.89%	2.75%
-10	0.71%	4.34%	0.58%	0.82%	3.73%	2.26%

From Table 3, it can be seen that the maximal relative error is less than 5%. The differences between the experimental and theoretical results are due to the fact that the mass of springs and the joint friction are not considered during the theoretical computation. However, the relative errors shown in Table 3 are acceptable in engineering.

5. Conclusion

Based on the analytical and experimental investigations presented in this paper, the following conclusions can be drawn:

1. On the basis of the Lagrangian formulation, we have derived the constraint equations which can be used to obtain the force-displacement relationship for a tensegrity structure. This method does not need any symmetry of the structure.

2. We have discussed bars' interferences that may occur in the real world. The interference conditions should be considered during finding the force-displacement relationships.

3. An experimental prototype has been made to certify the correctness of the obtained relationships between the external force applied on node B_3 along the Z axis and the extensions of the springs. The experimental results indicate that the force-displacement relationship obtained by the Lagrangian formulation are acceptable in engineering.

Acknowledgements

This research is supported by the National Natural Science Foundation of China (No.51375360).

Appendix A. Details of variables L_i

Using the notations $\vec{I}^3_1=\hat{I}\pm1\hat{a}\hat{I}_1$, $\vec{I}^3_2=\hat{I}\pm2\hat{a}\hat{I}_2$ and $\vec{I}^3_3=\hat{I}\pm3\hat{a}\hat{I}_3$, due to the symmetry of the spatial mechanism, the lengths L_1, L_2, L_3, L_4, L_5 and L_6 have, in fact, the following interesting expressions:

$$L_1^2 = L^2+a^2+2La\cos\vec{I}^2_1\cos(\hat{I}^3_2\hat{a}\ddot{I}/6) \tag{A.1}$$

$$L_2^2=L^2+a^2+2La\cos\vec{I}^2_3\cos(\vec{I}^3_3\hat{a}\ddot{I}/6) \tag{A.2}$$

$$L_3^2=L_2+a_2+2La\cos\vec{I}^2_1\cos(\vec{I}^3_1\hat{a}\ddot{I}/6) \tag{A.3}$$

$$L_4^2=2L^2+a^2+2\mathrm{La}\cos\vec{I}^2_1\cos(\vec{I}^3_1+\ddot{I}/6)+2La\cos\vec{I}^2_2\cos(\vec{I}^3_2\hat{a}\ddot{I}/6)+$$

$$2L^2\cos\vec{I}^2_1\cos\vec{I}^2_2\cos(\vec{I}^3_1\hat{a}\,\vec{I}^3_2+\ddot{I}/3)\hat{a}^2L^2\sin\vec{I}^2_1\sin\vec{I}^2_2 \tag{A.4}$$

$$L_5^2=2L^2+a^2+2\mathrm{La}\cos\vec{I}^2_1\cos(\vec{I}^3_2+\ddot{I}/6)+2La\cos\vec{I}^2_3\cos(\vec{I}^3_3\hat{a}\ddot{I}/6)+$$

$$2L^2\cos\vec{I}^2_2\cos\vec{I}^2_3\cos(\vec{I}^3_2\hat{a}\vec{I}^3_3+\ddot{I}/3)\hat{a}^2L^2\sin\vec{I}^2_2\sin\vec{I}^2_3 \tag{A.5}$$

$$L_6^2=2L^2+a^2+2La\cos\vec{I}^2_3\cos(\vec{I}^3_3+\ddot{I}/6)+2La\cos\vec{I}^2_1\cos\hat{I}^2_1\cos(\vec{I}^3_1\hat{a}\ddot{I}/6)+$$

$$2L_2\cos\vec{I}^2_3\cos\vec{I}^2_1\cos(\vec{I}^3_3\hat{a}\vec{I}^3_1+\ddot{I}/3)\hat{a}^2L_2\sin\vec{I}^2_3\sin\vec{I}^2_1 \tag{A.6}$$

REFERENCES

[1] *D. Cadoni and A. Micheletti*, "Structural performances of single-layer tensegrity domes", International Journal of Space Structures, Vol. 27, no. 2, 2012, pp. 167-178.

[2] *F. Fu*, "Structural behavior and design methods of tensegrity domes", Journal of Constructional Steel Research, Vol. 61, no. 1, 2005, pp. 23-35.

[3] *B. Gao, Q. Lu, and S. Dong*, "Geometrical nonlinear stability analyses of cable-truss domes", Journal of Zhejiang University Since A, Vol. 4, no. 3, 2003, pp. 317-323.

[4] *S. Pellegrino*, "A class of tensegrity domes", International Journal of Space Structures, Vol. 7, 1992, pp. 127-142.

[5] *L. Rhode-Barbarigos, N. B. H. Ali, R. Motro, R. and I. F. Smith*, "Designing tensegrity modules for pedestrian bridges", Engineering Structures Vol. 32, no. 4, 2010, pp. 1158-1167.

[6] *R. Skelton, F. Fraternali, G. Carpentieri and A. Micheletti*, "Minimum mass design of tensegrity bridges with parametric architecture and multiscale complexity", Mechanics Research Communications, Vol. 58, 2014, pp. 124-132.

[7] *C. Sultan and R. Skelton*, "A force and torque tensegrity sensor", Sensors and Actuators A: Physical, Vol. 112, no. 2, 2004, pp. 220-231.
[8] *N. Fazli and A. Abedian*, "Design of tensegrity structures for supporting deployable mesh antennas", Scientia Iranica, Vol. 18, no. 5, 2011, pp. 1078-1087.
[9] *B. F. Knight*, Deployable antenna kinematics using tensegrity structure design, PhD Thesis, University of Florida, 2004.
[10] *C. Paul, F. J. Valero-Cuevas and H. Lipson*, "Design and control of tensegrity robots for locomotion", IEEE Transactions on Robotics, Vol. 22, 2006, pp. 944-957.
[11] *A. G. Rovira and J. M. M. Tur*, "Control and simulation of a tensegrity-based mobile robot", Robotics and Autonomous Systems, Vol. 57, 2009, pp. 526-535.
[12] *M. Arsenault and C. M. Gosselin*, "Kinematic and static analysis of a three-degree-of-freedom spatial modular tensegrity mechanism", The International Journal of Robotics Research, Vol. 27, no. 8, 2008, pp. 951-966.
[13] *Z. Ji, T. Li, and M. Lin*, "Kinematics and stiffness of a planar tensegrity parallel mechanism", Periodica Polytechnica, Mechanical Engineering, Vol. 58, no.2, 2014, pp. 101-111.
[14] *Z. Ji, T. Li, and M. Lin*, "Kinematics, workspaces and stiffness of a planar class-2 tensegrity mechanism", U.P.B. Scientific Bulletin, Series D: Mechanical Engineering, **Vol. 76**, no. 3, 2014, pp. 53-64.
[15] *R. E. Vasquez, C. D. Crane and J. C. Correa*, "Analysis of a Planar Tensegrity Mechanism for Ocean Wave Energy Harvesting", Journal of Mechanisms and Robotics, Vol. 6, no. 3, 2014, pp. 031015.
[16] *A. Tibert, and S. Pellegrino*, "Review of form-finding methods for tensegrity structures", International Journal of Space Structures, Vol. 18, no. 4 2003, pp. 209-223.
[17] *M. Masic, R. E. Skelton and P. E. Gill*, "Algebraic tensegrity form-finding", International Journal of Solids and Structures, Vol. 42, no. 16, 2005, pp. 4833-4858.
[18] *M. Pagitz and J. M. Tur*, "Finite element based form-finding algorithm for tensegrity structures", International Journal of Solids and Structures, Vol. 46, no. 17, 2009, pp. 3235-3240.
[19] *S. H. Juan, and J. M. M. Tur*, "Tensegrity frameworks: static analysis review", Mechanism and Machine Theory, Vol. 43, no. 7, 2008, pp. 859-881.
[20] *N. Kanchanasaratool and D. Williamson*, "Modelling and control of class NSP tensegrity structures", International Journal of Control, Vol. 75, no. 2, 2005, pp. 123-139.
[21] *R. E. Skelton, J. P. Pinaud and D. Mingori*, "Dynamics of the shell class of tensegrity structures", Journal of the Franklin Institute, Vol. 338, no. 2, 2001, pp. 255-320.
[22] *R. Motro, S. Najari and P. Jouanna*, "Static and dynamic analysis of tensegrity systems", Shell and Spatial Structures: Computational Aspects, Proceedings of the International Symposium,1987, pp. 270-279.
[23] *H. Murakami*, "Static and dynamic analyses of tensegrity structures. Part 1. Nonlinear equations of motion", International Journal of Solids and Structures, Vol. 38, no. 20, 2001, pp. 3599-3613.
[24] *I. Oppenheim and W. Williams*, "Geometric effects in an elastic tensegrity structure", Journal of Elasticity, **Vol. 59**, no. 1, 2000, pp. 51-65.
[25] S. *Staicu*, "Matrix modeling of inverse dynamics of spatial and planar parallel robots", Multibody System Dynamics**, Vol. 27**, no. 2, 2012, pp. 239-265.